Editors' Suggestion

Nutational switching in ferromagnets and antiferromagnets

Lucas Winter, Sebastian Großenbach, Ulrich Nowak, and Levente Rózsa*
Fachbereich Physik, Universität Konstanz, DE-78457 Konstanz, Germany

(Received 18 July 2022; revised 21 October 2022; accepted 7 November 2022; published 5 December 2022)

It was demonstrated recently that on ultrashort timescales magnetization dynamics not only exhibits precession but also nutation. Here, we investigate how nutation can contribute to spin switching, leading towards ultrafast data writing. We use analytic theory and numerical spin simulations to discuss the behavior of ferromagnets and antiferromagnets in high-frequency magnetic fields. In ferromagnets, linearly polarized fields align the magnetization perpendicular to the external field, enabling 90° switching. For circularly polarized fields in the xy plane, the magnetization tilts to the z direction. During this tilting it rotates around the z axis, allowing 180° switching. In antiferromagnets, external fields with frequencies higher than the nutation frequency align the order parameter parallel to the field direction, while for lower frequencies it is oriented perpendicular to the field. The switching frequency increases with the magnetic field strength, and it deviates from the Larmor frequency, making it possible to outpace precessional switching in high magnetic fields.

DOI: 10.1103/PhysRevB.106.214403

I. INTRODUCTION

Deterministic spin switching plays an important role in industrial applications, for example, in magnetic memory devices [1–4]. However, as industrial needs exceed currently available switching speeds, the search for new physical effects that can accelerate spin switching is ongoing. One such pathway might be exploiting spin nutation. In spin nutation, the direction of the magnetic moment and angular momentum become separated on ultrashort timescales [5,6], and the magnetic moment rotates around the angular momentum [7]. Spin nutation is described by the inertial Landau-Lifshitz-Gilbert (ILLG) equation [5,6]. The ILLG equation extends the Landau-Lifshitz-Gilbert (LLG) equation by an additional inertial term containing a second-order time derivative of the magnetic moment. The inertial term originates from spin-orbit coupling, as it can be derived using the Dirac equation [8].

Linear-response theory applied to the ILLG equation predicts a spin nutation resonance in addition to the precession resonance in ferromagnets [9–11] and in antiferromagnets [12]. Recently the nutation resonance has been experimentally observed in ferromagnetic thin films [13]. Estimates for the angular momentum relaxation parameter η characterizing the nutation period range from the order of 1 fs [5,14–16] to several 100 fs [13,17]. Experiments in epitaxial cobalt films suggest that this parameter is proportional to the magnetocrystalline anisotropy [17], which similarly emerges due to the spin-orbit coupling.

For writing data in magnetic hard drives, usually a magnetic pulse with opposite direction to the magnetization is applied [18,19]. Subsequently, the damping switches the magnetization in approximately 100 ps. In this case, the damping constant limits the switching time [20]. Several authors have proposed faster switching mechanisms by using transverse magnetic field pulses [21,22]. In this case, the switching time depends on the energy delivered by the magnetic pulse. Tudosa *et al.* experimentally demonstrated ultrafast switching using magnetic field pulses [23]. Moreover, they argued that switching on a timescale shorter than 2 ps is impossible in ferromagnets. However, because of practical limitations, this lower bound has never been confirmed experimentally [23]. By using the intrinsic inertia of antiferromagnetic dynamics, it is possible to reduce switching times by a factor of 10 compared to ferromagnets [24]. The role of the extrinsic inertia as described by the ILLG equation for spin switching has hardly been studied so far, apart from a recent work by Neeraj *et al.* [25] which focused on applying a magnetic field pulse without an oscillating component. They showed that the inertial term opens an additional energy channel slightly modifying the switching time. However, it remains to be seen how a resonant excitation of the nutational motion influences the switching time. Since the nutation frequency is much higher than the precession frequency, it stands to reason that nutation could be advantageous for faster magnetization switching.

Here we investigate how terahertz magnetic fields can be utilized for spin switching in ferromagnets (FMs) and antiferromagnets (AFMs). We show that if the nutation is resonantly excited by the magnetic field, it exerts a torque on the order parameter, reorienting its direction. We discuss nutational switching modes analytically by proposing an alternative form of the ILLG equation based on the angular momentum and numerically by using spin simulations. It is found that a linearly polarized magnetic field enables a 90° switching mode of the order parameter. A circularly polarized field initiates the tilting of the order parameter from the equilibrium direction earlier than the linearly polarized field, and it can also be used for 180° spin switching. The switching time is found to be around 20 ps in FMs and around 5 ps in AFMs. It is demonstrated that the switching velocity of nutational switching is

*Corresponding author: levente.rozsa@uni-konstanz.de

by a factor of 2 higher than that of precessional switching in a wide parameter range.

The paper is organized as follows. In Sec. II we treat nutational switching analytically and propose an alternative representation of the ILLG equation using the angular momentum. In this representation we discuss nutational switching in FMs in Sec. III both by linearly and by circularly polarized fields. Using numerical spin simulations, we show that linearly polarized fields can be used for 90° switching and circularly polarized fields for 180° switching. We investigate nutational switching in AFMs in Sec. IV. We determine the switching time for a wide range of material parameters and compare it to the switching time in FMs and to precessional switching.

II. THEORY OF NUTATIONAL SWITCHING

The dynamics of the magnetic moments will be described using the ILLG equation as derived in earlier works [5,8,14], reading

$$\dot{\boldsymbol{M}}_i = -\gamma_i \boldsymbol{M}_i \times \mu_0 \boldsymbol{H}_{\mathrm{eff},i} + \frac{\alpha_i}{M_{0,i}} \boldsymbol{M}_i \times \dot{\boldsymbol{M}}_i + \frac{\eta_i}{M_{0,i}} \boldsymbol{M}_i \times \ddot{\boldsymbol{M}}_i. \tag{1}$$

The first term in Eq. (1) describes precession with the gyromagnetic ratio γ_i and the second term transversal relaxation with damping constant α_i. The third term induces inertial dynamics with inertial relaxation time η_i. Here, i enumerates the magnetic moments, taking into account possible deviations in the gyromagnetic ratio and the relaxation time between different sublattices. In general, α_i and η_i are tensors. In this work we consider α_i and η_i as scalar quantities [8], which is allowed in all symmetry groups. $M_{0,i}$ is the magnitude of the magnetic moment, and $\boldsymbol{H}_{\mathrm{eff},i}$ denotes the effective field $\boldsymbol{H}_{\mathrm{eff},i} = -\frac{1}{\mu_0}\frac{\partial \mathcal{H}}{\partial \boldsymbol{M}_i}$, where $\mathcal{H} = \mathcal{H}_{\mathrm{exch}} + \mathcal{H}_{\mathrm{ani}} - \sum_i \mu_0 \boldsymbol{M}_i[\boldsymbol{H}_{\mathrm{ext}} + \boldsymbol{H}_{\mathrm{osc}}(t)]$ is the Hamiltonian of the system containing exchange $\mathcal{H}_{\mathrm{exch}}$ and anisotropy $\mathcal{H}_{\mathrm{ani}}$ energy, as well as static $\boldsymbol{H}_{\mathrm{ext}}$ and oscillating $\boldsymbol{H}_{\mathrm{osc}}$ external field terms. The $\mathcal{H}_{\mathrm{exch}}$ and $\mathcal{H}_{\mathrm{ani}}$ terms will be specified in Secs. III and IV for FMs and AFMs, respectively. In the simulations, we solve the ILLG equation numerically using the implementation of Heun's method described in Ref. [12]. As Heun's method does not preserve the spin length, $\boldsymbol{M}_i$ is normalized in every simulation step.

Because of the inertial term, the angular momentum $\boldsymbol{L}_i$ is no longer parallel to the magnetic moment $\boldsymbol{M}_i$ as in the LLG equation [5], leading to

$$\boldsymbol{L}_i = \frac{1}{\gamma_i}\boldsymbol{M}_i - \Delta\boldsymbol{L}_i. \tag{2}$$

Here we introduced the nutation vector $\Delta\boldsymbol{L}_i = \frac{\eta_i}{M_{0,i}\gamma_i}\boldsymbol{M}_i \times \dot{\boldsymbol{M}}_i$ for this deviation. Equation (2) represents an out-of-equilibrium connection between angular momentum $\boldsymbol{L}_i$ and magnetization $\boldsymbol{M}_i$ [5]. The configuration space containing the magnetic moment directions $\boldsymbol{M}_i$ is extended by the degrees of freedom of the angular momentum $\boldsymbol{L}_i$ in the phase space. The vectors $\boldsymbol{L}_i, \boldsymbol{M}_i$, and $\Delta\boldsymbol{L}_i$ are illustrated in Fig. 1(a). Note that for simplicity we used a sign convention where without the inertial term $\boldsymbol{L}_i$ is pointing along $\boldsymbol{M}_i$ ($\gamma_i > 0$), although Eq. (1) describes the time evolution of electronic spins. The nutation amplitude $|\Delta\boldsymbol{L}_i|$ is usually much smaller than the angular momentum amplitude, because $|\Delta\boldsymbol{L}_i| = |\frac{\eta_i}{\gamma_i M_{0,i}}\boldsymbol{M}_i \times \dot{\boldsymbol{M}}_i| \approx \frac{\eta_i}{M_{0,i}}|\boldsymbol{M}_i \times (\boldsymbol{M}_i \times \mu_0 \boldsymbol{H}_{\mathrm{eff},i})| \leqslant \gamma_i \eta_i \mu_0 |\boldsymbol{H}_{\mathrm{eff},i}||\boldsymbol{L}_i|$ and $\gamma_i \eta_i \mu_0 |\boldsymbol{H}_{\mathrm{eff},i}| \ll 1$, even for relatively large inertial relaxation times of $\eta_i \approx 100$ fs.

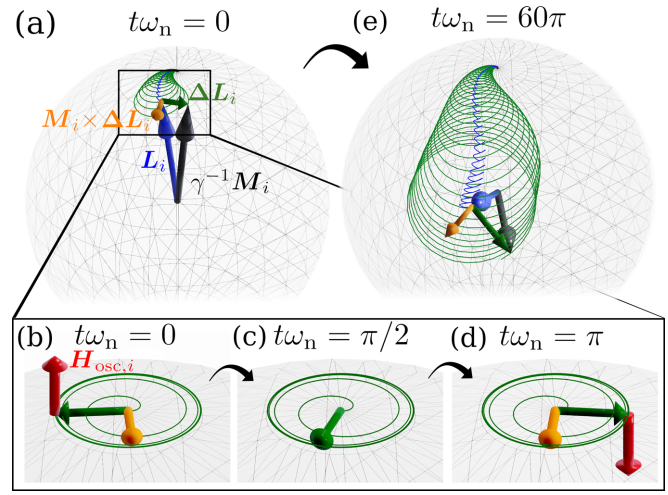

FIG. 1. Illustration of nutational switching. (a) First, an oscillating magnetic field $\boldsymbol{H}_{\mathrm{osc}}$ is applied to a magnetic moment $\boldsymbol{M}_i$. (b)–(d) This excites a finite nutation amplitude $\Delta\boldsymbol{L}_i$. (e) The nutation vector in conjunction with the external field exerts a torque proportional to $\langle \Delta\boldsymbol{L}_i \times \boldsymbol{H}_{\mathrm{osc}} \rangle_t$.

For understanding the nutation-induced switching, we decompose the magnetic moment using the angular momentum $\boldsymbol{L}_i$ and the nutation $\Delta\boldsymbol{L}_i$ according to $\boldsymbol{M}_i = \gamma(\boldsymbol{L}_i + \Delta\boldsymbol{L}_i)$. The ILLG equation becomes a system of coupled first-order differential equations,

$$\dot{\boldsymbol{L}}_i = -\gamma_i \boldsymbol{L}_i \times \mu_0 \boldsymbol{H}_{\mathrm{eff},i} - \gamma_i \Delta\boldsymbol{L}_i \times \mu_0 \boldsymbol{H}_{\mathrm{eff},i} + \frac{\alpha_i}{\eta_i}\Delta\boldsymbol{L}_i, \tag{3}$$

$$\Delta\dot{\boldsymbol{L}}_i = \gamma_i \Delta\boldsymbol{L}_i \times \left(\frac{1}{M_{0,i}\eta_i}\boldsymbol{L}_i + \mu_0 \boldsymbol{H}_{\mathrm{eff},i}\right) + \gamma_i \boldsymbol{L}_i \times \mu_0 \boldsymbol{H}_{\mathrm{eff},i} - \frac{\alpha_i}{\eta_i}\Delta\boldsymbol{L}_i; \tag{4}$$

see Appendix A for the derivation.

We will analyze these differential equations in the following, starting with a qualitative understanding of nutational switching. A field $\boldsymbol{H}_{\mathrm{osc}}$ oscillating at the nutation frequency $\omega = \omega_{\mathrm{n}}$ is applied to the magnetic moment, as shown in Fig. 1(a). As a consequence, the magnetic moment starts to nutate with finite nutation amplitude. Linear-response theory predicts nutation with the same frequency as $\boldsymbol{H}_{\mathrm{osc}}$ and a finite phase shift. However, according to Eq. (3), $\Delta\boldsymbol{L}_i$ will interact with the oscillating field $\boldsymbol{H}_{\mathrm{osc}}$ and exert a torque $-\gamma\Delta\boldsymbol{L}_i \times \mu_0 \boldsymbol{H}_{\mathrm{osc}}$ on the angular momentum $\boldsymbol{L}_i$. Figure 1(b) shows the direction of the torque. Because of the constant phase difference between $\Delta\boldsymbol{L}_i$ and $\boldsymbol{H}_{\mathrm{osc}}$, the torque still points in the same direction after half a nutation period; see Fig. 1(d). This means that the torque has a finite time average that drives the switching, as shown in Fig. 1(e). This torque only arises

at very short timescales where the directions of $\boldsymbol{L}_i$ and $\boldsymbol{M}_i$ are separated, giving rise to a finite nutation amplitude.

Theoretical estimates [5,14–16] supported by recent experimental evidence [13,17] suggest that the nutation frequency η_i^{-1} is much higher than the precession frequency. This allows for a separation of timescales between the fast variable $\Delta\boldsymbol{L}_i$ and the slow variable $\boldsymbol{L}_i$. We define a coordinate system where the angular momentum is oriented along the radial direction in spherical coordinates $\boldsymbol{L}_i = L_{0,i} \cdot \hat{\mathbf{e}}_{r,i}$. The nutation is then essentially a two-dimensional motion happening in the plane perpendicular to the angular momentum as the nutation amplitude is usually small. We introduce the complex amplitude $c_i(t)$ for the nutation vector $\Delta\boldsymbol{L}_i$, with $\Delta\boldsymbol{L}_i = \mathrm{Re}\{c_i(t)\}\hat{\mathbf{e}}_{\vartheta,i} + \mathrm{Im}\{c_i(t)\}\hat{\mathbf{e}}_{\varphi,i}$ in the coordinate system defined by the angular momentum. This allows for finding an instantaneous solution for the nutation amplitude $c_i(t)$ in a linear-response framework; see Appendix B.

For a single macrospin, we can give the closed-form solution for $\boldsymbol{H}_{\mathrm{eff}}(t,\vartheta,\varphi) = \boldsymbol{H}_0(\vartheta,\varphi) + \boldsymbol{H}_{\mathrm{osc}}(t,\vartheta,\varphi)$, a sum of a time-dependent oscillating field $\boldsymbol{H}_{\mathrm{osc}} = \boldsymbol{h}e^{-i\omega t} + \boldsymbol{h}^* e^{i\omega t}$ with complex amplitude $\boldsymbol{h}$, and a time-independent external field $\boldsymbol{H}_0(\vartheta,\varphi)$ which contains the external Zeeman field $\boldsymbol{H}_{\mathrm{ext}}$ and anisotropy $\boldsymbol{H}_{\mathrm{ani}}$. The contribution of $\boldsymbol{H}_{\mathrm{osc}}$ to ω_{n} is neglected in the linear-response regime. From now on we will not explicitly write the orientation dependence (ϑ,φ). With these notations one obtains

$$c(t) = c_{\mathrm{hom}}(t) - \mu_0 M_0(\hat{\mathbf{e}}_\varphi - i\hat{\mathbf{e}}_\vartheta)\cdot\left(\frac{e^{-i\omega t}}{i(\omega_{\mathrm{n}}-\omega)+\alpha/\eta}\boldsymbol{h} + \frac{e^{i\omega t}}{i(\omega_{\mathrm{n}}+\omega)+\alpha/\eta}\boldsymbol{h}^* + \frac{1}{i\omega_{\mathrm{n}}+\alpha/\eta}\boldsymbol{H}_0\right), \tag{5}$$

with the homogeneous solution $c_{\mathrm{hom}} = c_0 e^{-\frac{i}{\eta}t} e^{-\frac{\alpha}{\eta}t}$. For $t \gg \eta/\alpha$, the homogeneous solution will become negligible. In this case the nutation is a circular motion with the frequency ω of the external field and a resonance at $\omega = \omega_{\mathrm{n}}$. Moreover, the anisotropy and the constant magnetic field are responsible for a constant offset of the nutation amplitude. This offset leads to the relaxation of the magnetic moment towards the direction of the angular momentum.

Using Eqs. (4) and (5), it is now possible to discuss the time evolution of the angular momentum $\boldsymbol{L}$ taking place on longer timescales. We can express the change in angular momentum (3) using the nutation vector $\Delta\boldsymbol{L}$ as

$$\langle\dot{\boldsymbol{L}}\rangle_t = -\langle\gamma\boldsymbol{L}\times\mu_0\boldsymbol{H}_{\mathrm{eff}}\rangle_t + \left\langle\frac{\alpha}{\eta}\Delta\boldsymbol{L}\right\rangle_t - \langle\gamma\,\Delta\boldsymbol{L}\times\mu_0\boldsymbol{H}_{\mathrm{eff}}\rangle_t, \tag{6}$$

where $\langle\cdot\rangle_t$ indicates time averaging over one nutation period. The first term in Eq. (6) is the precession term, which is functionally unchanged from the LLG equation. The second term in Eq. (6) is responsible for the damping. In this representation, the damping is closely linked with the nutation amplitude. For a more detailed explanation see Appendix C. The third term in Eq. (6), $-\langle\gamma\,\Delta\boldsymbol{L}\times\mu_0\boldsymbol{H}_{\mathrm{eff}}\rangle_t$, only appears because of inertial effects. This term is responsible for the nutational switching.

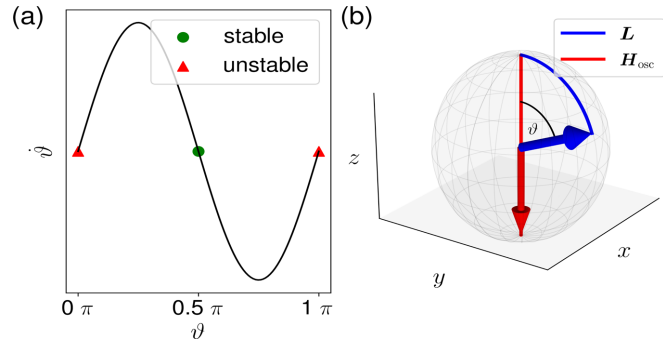

FIG. 2. Illustration of the nutational switching mode in FMs for a linearly polarized field. (a) Dependence of the right-hand side of Eq. (7) on ϑ. The stationary point $\vartheta = \pi/2$ is stable, $\vartheta = 0, \pi$ are unstable. (b) Illustration of the solution of the differential equation (7). The linearly polarized field along the z axis tilts the spin towards the y direction.

III. NUTATIONAL SWITCHING IN FERROMAGNETS

A. Nutational switching for linearly polarized fields

For an easier interpretation, we will neglect the precession and damping terms in Eq. (6) in the following. Damping effects are not completely neglected, as they are still present in the solution for the nutation amplitude $\Delta\boldsymbol{L}$ in Eq. (5). We describe the time evolution of $\boldsymbol{L}$ on this longer timescale in spherical coordinates, where ϑ represents the angle between $\boldsymbol{L}$ and the z axis, and φ represents the angle measured from the x axis in the xy plane. The closed-form solution for $\Delta\boldsymbol{L}$ in Eq. (5) can be expressed in spherical coordinates using $\Delta\boldsymbol{L} = \mathrm{Re}\{c(t)\}\hat{\mathbf{e}}_\vartheta + \mathrm{Im}\{c(t)\}\hat{\mathbf{e}}_\varphi$.

For a linearly polarized field $\boldsymbol{H}_{\mathrm{osc}} = h\hat{\mathbf{e}}_z\cos(\omega t)$, Eq. (6) can be expressed as

$$\dot{\vartheta} = \frac{1}{2}\left(\frac{\gamma\mu_0 h}{2}\right)^2 \frac{\alpha/\eta}{(\omega_{\mathrm{n}}-\omega)^2 + \frac{\alpha^2}{\eta^2}}\sin(2\vartheta). \tag{7}$$

For an illustration of the right-hand side of Eq. (7), see Fig. 2(a). There are three stationary points. $\vartheta = 0$ and $\vartheta = \pi$ are unstable. In these cases the spin is either parallel or antiparallel to the magnetic field, but any small perturbation will tilt it away from these directions. The point $\vartheta = \pi/2$ is stable. In this case the spin is perpendicular to the magnetic field. If the spin is not in one of these three configurations, it will align itself perpendicular to the field at $\vartheta = \pi/2$, as shown in Fig. 2(b). This type of switching is shown in Supplemental Video 1 [26].

From Eq. (7) it follows that the tilting velocity is highest at the nutation resonance $\omega = \omega_{\mathrm{n}}$. Materials with high values of η and low values of α should exhibit the highest tilting speeds. Moreover, the tilting velocity increases with increasing magnetic field, and the magnetic moment will align perpendicular to a linearly polarized magnetic field. In a system with cubic anisotropy $\mathcal{H}_{\mathrm{ani}} = -K_4(M_x^4 + M_y^4 + M_z^4)/M_0^4$ with potential minima separated by an angle of 90°, applying the field along the magnetization direction should enable 90° switching. Such a switching would be possible to detect by measuring the magnetization direction or through the anisotropic magnetoresistance.

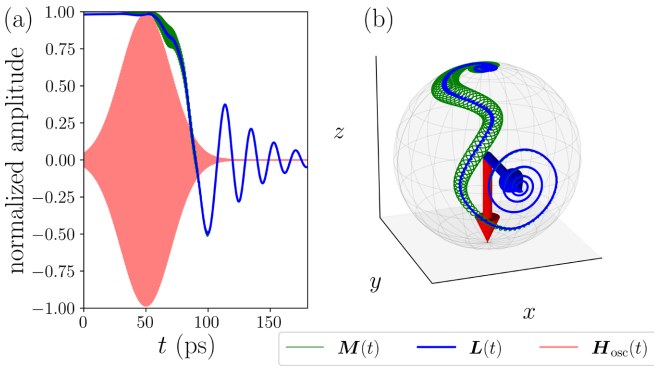

FIG. 3. 90° switching using a linearly polarized field along the z direction. The material parameters are $\alpha = 0.1$, $\eta = 100$ fs, $M_0 = 2\mu_B$ and a cubic anisotropy with $K_4 = 10^{-23}$ J. The magnetic field strength is $\mu_0 h = 5$ T, the field frequency is $\omega = \omega_n = 1 \times 10^{13}$ s^{-1}, and the pulse width is $\sigma = 20$ ps.

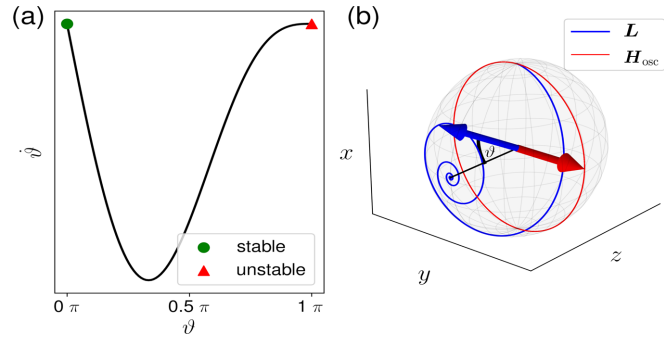

FIG. 4. Illustration of the nutational switching mode in FMs for a circularly polarized field. (a) Dependence of the right-hand side of Eq. (8) on ϑ. The stationary point $\vartheta = 0$ is stable, $\vartheta = \pi$ is unstable. (b) Illustration of the solution to the differential equations (8) and (9). In the beginning, the magnetic moment points along the x direction.

We use numerical spin simulations to validate this prediction and start with a single macrospin aligned close to the z direction. We then apply a magnetic field pulse along the z direction at the nutation frequency $\omega = \omega_n \approx \frac{1}{\eta}$ with a Gaussian pulse shape given by $\boldsymbol{H}_{osc} = h \exp(-\frac{(t-t_0)^2}{2\sigma^2})\hat{\mathbf{e}}_z \cos(\omega t)$, where σ is the pulse width and t_0 is the pulse center. As shown in Fig. 3, the behavior of the magnetic moment in the simulations is consistent with the analytic prediction shown in Fig. 2 but superimposed with a precession caused by the anisotropy term. Here, the switching was achieved with a pulse width of $\sigma = 20$ ps. The tilting speed itself is high, as it takes only 23 ps for L_z to decay to $1/e$ of its initial value. If the magnetic field is turned off at this point, one can be sure that the magnetic moment will relax to the switched position, since it has already crossed the anisotropy energy barrier at $\vartheta = \pi/4$. However, it takes a significant amount of time for the tilting to start, because a magnetic field almost parallel to the magnetic moment excites the nutation slowly according to Eq. (7). Applying the linearly polarized field at a small angle from the initial equilibrium direction could likely decrease the switching time. Moreover, finite temperature would likely alleviate this problem, because there the spin would not be exactly parallel to the external field.

B. Nutational switching for circularly polarized fields

For a circularly polarized field $\boldsymbol{H}_{osc} = h[\cos(\omega t)\ \hat{\mathbf{e}}_x + \sin(\omega t)\ \hat{\mathbf{e}}_y]$, Eq. (6) can be expressed in spherical coordinates as

$$\dot{\vartheta} = -\frac{(\gamma\mu_0 h)^2}{4}\frac{\alpha/\eta}{(\omega_n-\omega)^2+\frac{\alpha^2}{\eta^2}}\left(\sin(\vartheta)+\frac{1}{2}\sin(2\vartheta)\right), \tag{8}$$

$$\dot{\varphi} = -\frac{(\gamma\mu_0 h)^2}{2}\frac{\omega_n-\omega}{(\omega_n-\omega)^2+\frac{\alpha^2}{\eta^2}}(1+\cos(\vartheta)). \tag{9}$$

Equation (8) decouples from Eq. (9). Equation (9) shows that the angular momentum rotates around the z axis. The sense of rotation depends on whether the frequency of the external field is higher or lower than the nutation frequency. In resonance, $\omega = \omega_n$, the rotation around the z axis vanishes. The maximal rotation frequency is achieved for $\omega = \omega_n \pm \alpha/\eta$.

Figure 4(a) shows the right side of Eq. (8). There are two stationary points. First, we can see that $\vartheta = 0$ is stable, as the derivative on the right-hand side is negative. The point $\vartheta = \pi$ is unstable against perturbations. For all other angles, the magnetic moment rotates to align itself parallel to the z direction. As for linearly polarized magnetic fields, the speed is proportional to h^2. In resonance the tilting velocity is maximal. This type of switching is illustrated in Fig. 4(b) and Supplemental Video 2 [26].

The rotation around the z axis can also be used for 180° switching along the x or y axis. In this case it is useful to maximize the rotation frequency $\dot{\varphi}$ and minimize the tilting speed. Because $\dot{\varphi}/\dot{\vartheta} \propto \frac{\eta(\omega_n-\omega)}{\alpha}$, it is beneficial to consider a system with low damping and an excitation frequency above the nutation frequency. Circularly polarized fields could also be used for 90° switching, using the tilting mechanism similarly to linearly polarized fields. In this case, the ratio $\dot{\varphi}/\dot{\vartheta}$ should be minimized.

We use numerical spin simulations to validate the analytical results. We apply a circularly polarized field in the xy plane to a single macrospin. At $t = 0$ s the spin is aligned with the y axis, selected by a uniaxial anisotropy term $\mathcal{H}_{ani} = -\frac{K_y}{M_0^2}M_y^2$, facilitating 180° switching. We apply an external field frequency above the nutation frequency and a smaller α value than in the linearly polarized case to maximize the ratio $\dot{\varphi}/\dot{\vartheta}$.

As shown in Fig. 5, the behavior of the magnetization in the simulations is consistent with the analytical prediction shown in Fig. 4(b). The nutation amplitude is much larger than in the linearly polarized case because α is smaller. Switching is possible with a pulse width of $\sigma = 10$ ps, significantly shorter than for linearly polarized fields. For a system with weaker anisotropy, even shorter pulses could be used. The switching starts significantly earlier than in the linearly polarized case because a nutation amplitude is excited much quicker. While a linearly polarized field parallel to the angular momentum does not lead to nutation, a circularly polarized field can excite a nutation in any orientation, according to Eq. (4).

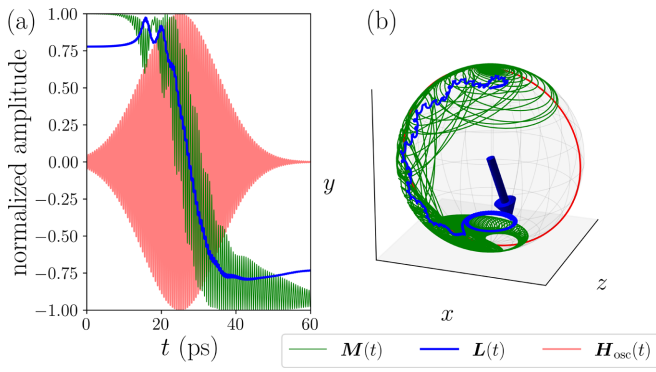

FIG. 5. 180° switching using a circularly polarized field in the xy plane. The material parameters are $\alpha = 0.01$, $\eta = 100$ fs, $M_0 = 2\mu_B$, and a uniaxial anisotropy with $K_y = 10^{-23}$ J along the y axis. The magnetic field strength is $\mu_0 h = 5$ T, the field frequency is $\omega = 1.1 \times 10^{13}$ s^{-1}, and the pulse width is $\sigma = 10$ ps.

IV. NUTATIONAL SWITCHING IN ANTIFERROMAGNETS

A. Analytical model

In addition to the extrinsic inertial term η_i of the ILLG equation, AFMs possess additionally an intrinsic inertia due to the exchange coupling between the two sublattices. This can be expected to have an impact on nutational switching.

In AFMs the order parameter is the staggered magnetization $\boldsymbol{N} = \boldsymbol{M}_A - \boldsymbol{M}_B$. We can decompose this into a staggered nutation $\Delta\boldsymbol{L}_N = \Delta\boldsymbol{L}_A - \Delta\boldsymbol{L}_B$ and a staggered angular momentum $\boldsymbol{L}_N = \boldsymbol{L}_A - \boldsymbol{L}_B$ with $\boldsymbol{N} = \gamma(\boldsymbol{L}_N + \Delta\boldsymbol{L}_N)$. As in FMs, the nutation vector of the sublattices can be represented by scalar complex variables c_A and c_B with $\Delta\boldsymbol{L}_A = \mathrm{Re}\{c_A\}\hat{\mathbf{e}}_{\vartheta,A} + \mathrm{Im}\{c_A\}\hat{\mathbf{e}}_{\varphi,A}$ and $\Delta\boldsymbol{L}_B = \mathrm{Re}\{c_B\}\hat{\mathbf{e}}_{\vartheta,B} + \mathrm{Im}\{c_B\}\hat{\mathbf{e}}_{\varphi,B}$. The Hamiltonian contains the exchange term $\mathcal{H}_{\mathrm{exch}} = \frac{J}{M_0^2}\boldsymbol{M}_A \cdot \boldsymbol{M}_B$, where $J > 0$ describes the AFM coupling between the sublattices. The nutation amplitude in linear response to the oscillating field $\boldsymbol{H}_{\mathrm{osc}} = \boldsymbol{h}e^{-i\omega t} + \boldsymbol{h}^* e^{i\omega t}$ for weak antiferromagnetic coupling, $J \ll 2\frac{M_0}{\gamma\eta}$, is then given by

$$c_A = -\mu_0 M_0(\hat{\mathbf{e}}_\varphi - i\hat{\mathbf{e}}_\vartheta) \cdot \left(\frac{\boldsymbol{h}e^{-i\omega t}}{i(\omega_{\mathrm{n},A} - \omega) + \frac{\alpha}{\eta}} + \frac{\boldsymbol{h}^* e^{i\omega t}}{i(\omega_{\mathrm{n},A} + \omega) + \frac{\alpha}{\eta}} + \frac{\boldsymbol{H}_{0,A}}{i\omega_{\mathrm{n},A} + \frac{\alpha}{\eta}} \right), \tag{10}$$

$$c_B = \mu_0 M_0(\hat{\mathbf{e}}_\varphi + i\hat{\mathbf{e}}_\vartheta) \cdot \left(\frac{\boldsymbol{h}e^{-i\omega t}}{i(\omega_{\mathrm{n},B} - \omega) + \frac{\alpha}{\eta}} + \frac{\boldsymbol{h}^* e^{i\omega t}}{i(\omega_{\mathrm{n},B} + \omega) + \frac{\alpha}{\eta}} + \frac{\boldsymbol{H}_{0,B}}{i\omega_{\mathrm{n},B} + \frac{\alpha}{\eta}} \right), \tag{11}$$

with $\omega_{\mathrm{n},A/B} = \sqrt{1 + 2J\eta\gamma/M_0}/\eta \pm \gamma\hat{\mathbf{e}}_r \cdot \boldsymbol{H}_{\mathrm{ext}}$, where the $+$ sign is taken for the A sublattice and the $-$ sign for the B sublattice; see Appendix D for the derivation. In Eqs. (10) and (11) the influence of the antiferromagnetic coupling only enters in the form of a renormalized nutation frequency. The nutation frequency is identical to previous results obtained using linear-response theory [12].

By using Eq. (3) in conjunction with the solution for the nutation vectors Eqs. (10) and (11), we can derive a differential equation describing the order parameter $\boldsymbol{N}$. The derivation can be found in Appendix E. The second-order differential equation for the order parameter is

$$\begin{aligned}\boldsymbol{N} \times \ddot{\boldsymbol{N}} = &-\gamma[2(\boldsymbol{N} \cdot \mu_0\boldsymbol{H}_M)\dot{\boldsymbol{N}} - \boldsymbol{N} \times (\dot{\boldsymbol{H}}_M \times \boldsymbol{N})] \\ &- \gamma^2(\boldsymbol{N} \cdot \mu_0\boldsymbol{H}_M)(\boldsymbol{N} \times \mu_0\boldsymbol{H}_M) + \frac{\gamma^2 J}{4}\boldsymbol{N} \times \mu_0\boldsymbol{H}_N \\ &+ \frac{d}{dt}(\boldsymbol{N} \times \boldsymbol{T}_N) - \frac{\gamma J}{4}\boldsymbol{T}_M + \gamma(\boldsymbol{N} \times \boldsymbol{T}_N) \times \mu_0\boldsymbol{H}_M,\end{aligned} \tag{12}$$

where $\boldsymbol{T}_M = \gamma(\partial_t + \frac{\alpha}{\eta})(\Delta\boldsymbol{L}_A + \Delta\boldsymbol{L}_B)$ and $\boldsymbol{T}_N = \gamma(\partial_t + \frac{\alpha}{\eta})\Delta\boldsymbol{L}_N$. $\boldsymbol{H}_M = (\boldsymbol{H}_A + \boldsymbol{H}_B)/2$ contains, for example, the Zeeman field, whereas $\boldsymbol{H}_N = (\boldsymbol{H}_A - \boldsymbol{H}_B)/2$ takes the anisotropy into account. $\boldsymbol{H}_A$ and $\boldsymbol{H}_B$ are the effective fields acting on the sublattices excluding the exchange interaction.

The last three terms in Eq. (12) describe the influence of a finite nutation amplitude $\Delta\boldsymbol{L}_N$ on the dynamics. According to Eqs. (10) and (11), the total torque exerted by the nutation $\boldsymbol{T}_N = \boldsymbol{T}_{N,0} + \boldsymbol{T}_{N,\mathrm{osc}}(t)$ consists of a time-independent part $\boldsymbol{T}_{N,0}$, driven by the Zeeman field and the anisotropy, and an oscillating time-dependent part $\boldsymbol{T}_{N,\mathrm{osc}}(t)$, driven by the oscillating external field. For the first two terms we find

$$\left\langle \frac{d}{dt}(\boldsymbol{N} \times \boldsymbol{T}_N) - \frac{\gamma J}{4}\boldsymbol{T}_M \right\rangle_t = \left\langle \frac{d}{dt}(\boldsymbol{N} \times \boldsymbol{T}_{N,0}) - \frac{\gamma J}{4}\boldsymbol{T}_{M,0} \right\rangle_t. \tag{13}$$

The quickly changing contribution $\boldsymbol{T}_{N,\mathrm{osc}}(t)$ vanishes under time averaging. Therefore this term describes damping effects in constant magnetic fields or under the influence of anisotropy, and it is irrelevant for nutational switching, similarly to the term $\langle\frac{\alpha}{\eta}\Delta\boldsymbol{L}\rangle_t$ in Eq. (6). Nutational switching is only described by the last term in Eq. (12), which is analogous to $\langle\gamma\,\Delta\boldsymbol{L} \times \mu_0\boldsymbol{H}_{\mathrm{eff}}\rangle_t$ in Eq. (6). For further analyzing the impact of nutation on the order parameter, we will neglect all other terms. The second derivative $\ddot{\boldsymbol{N}}$ is then given by

$$\ddot{\boldsymbol{N}} \cdot \hat{\mathbf{e}}_\vartheta = -M_0\gamma\mu_0^2\left(\hat{\mathbf{e}}_\vartheta \cdot \frac{\omega(\omega_{\mathrm{n}} - \omega)\boldsymbol{H}_{\mathrm{osc}} + \frac{\alpha}{\eta}\dot{\boldsymbol{H}}_{\mathrm{osc}}}{(\omega_{\mathrm{n}} - \omega)^2 + \frac{\alpha^2}{\eta^2}}\right)\hat{\mathbf{e}}_r \cdot \boldsymbol{H}_{\mathrm{osc}}, \tag{14}$$

$$\ddot{\boldsymbol{N}} \cdot \hat{\mathbf{e}}_\varphi = -M_0\gamma\mu_0^2\left(\hat{\mathbf{e}}_\varphi \cdot \frac{\omega(\omega_{\mathrm{n}} - \omega)\boldsymbol{H}_{\mathrm{osc}} + \frac{\alpha}{\eta}\dot{\boldsymbol{H}}_{\mathrm{osc}}}{(\omega_{\mathrm{n}} - \omega)^2 + \frac{\alpha^2}{\eta^2}}\right)\hat{\mathbf{e}}_r \cdot \boldsymbol{H}_{\mathrm{osc}}, \tag{15}$$

see Appendix F for the derivation. Here we neglected the influence of the Zeeman field on the nutation frequency, meaning $\omega_{\mathrm{n},A} = \omega_{\mathrm{n},B} = \omega_{\mathrm{n}}$. This is justified, as $|\hat{\mathbf{e}}_r \cdot \boldsymbol{H}_{\mathrm{osc}}| \leqslant \omega_{\mathrm{p}} \ll \omega_{\mathrm{n}}$. In Eqs. (14) and (15), two different kinds of inertia appear. On the left-hand side, the second time derivative of the order parameter $\boldsymbol{N}$ indicates inertia due to the antiferromagnetic exchange coupling. The consequence of this type of inertia is that the order parameter can keep rotating even if no external torque is acting on it, since the energy can be transformed between the exchange and anisotropy terms [27]. Nutational inertia is found on the right-hand side. Energy can be pumped into the nutation amplitude by applying a terahertz magnetic

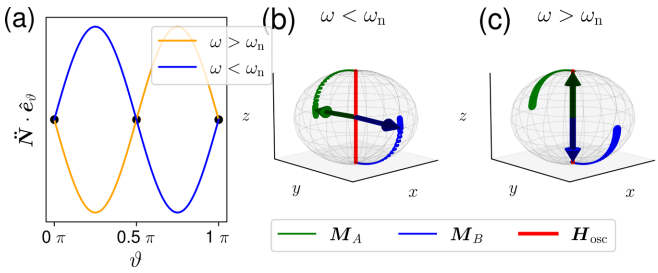

FIG. 6. Illustration of the nutational switching mode in AFMs for a linearly polarized field. (a) The right-hand side of Eq. (16) as a function of ϑ. (b, c) Illustrations of the switching modes when applying a linearly polarized magnetic field to AFMs for external field frequencies ω (b) below and (c) above the nutation frequency ω_n.

field. Then the finite nutation amplitude exerts a torque on the order parameter. Similarly to FMs, Eqs. (14) and (15) show that if the order parameter is perpendicular to the external field, the orientation is stable or unstable. We will further analyze Eqs. (14) and (15) for linearly and circularly polarized fields.

B. Nutational switching for linearly polarized fields

Next we investigate the behavior of the order parameter $\boldsymbol{N}$ in a linearly polarized magnetic field along the z axis, $\boldsymbol{H}_{\rm osc} = h\cos(\omega t)\hat{\mathbf{e}}_z$. For this purpose we substitute the magnetic field in Eqs. (14) and (15). For the $\hat{\mathbf{e}}_\vartheta$ component of $\ddot{\boldsymbol{N}}$ we find

$$\ddot{\boldsymbol{N}} \cdot \hat{\mathbf{e}}_\vartheta = \frac{\gamma^2 \mu_0^2 h^2}{8} \frac{\omega(\omega_n - \omega)}{(\omega_n - \omega)^2 + \frac{\alpha^2}{\eta^2}} \sin(2\vartheta). \tag{16}$$

Figure 6(a) shows an illustration of the right-hand side of Eq. (16). If the external frequency ω is smaller than the nutation frequency ω_n, the order parameter is stable if it is perpendicular to the external field at $\vartheta = \pi/2$. $\boldsymbol{N}$ is unstable if it is aligned with the external field at $\vartheta = 0$ or $\vartheta = \pi$. Consequently, the order parameter aligns itself perpendicular to the external field. The qualitative behavior is the same as for FMs. Figure 6(b) shows an illustration of this switching mode. For $\omega > \omega_n$ the parallel orientation $\vartheta = 0, \pi$ is stable and the perpendicular orientation $\vartheta = \pi/2$ is unstable. Therefore the order parameter aligns itself along the external field. Figure 6(c) shows an illustration of the latter switching mode. Differently to FMs, there are two different switching modes depending on the frequency of the external field $\boldsymbol{H}_{\rm osc}$. These switching modes are also shown in Supplemental Video 3 [26].

For a linearly polarized field along the z direction, from Eq. (15) immediately follows $\dot{\boldsymbol{N}} \cdot \hat{\mathbf{e}}_\varphi = 0$. Therefore, nutation for linearly polarized fields only leads to tilting but not to a rotation around the z direction.

Compared to the ferromagnetic case, there is also a different dependence on the material parameters. For $\alpha \to 0$ we get $\frac{\omega_n - \omega}{(\omega_n - \omega)^2 + \frac{\alpha^2}{\eta^2}} \to (\omega_n - \omega)^{-1}$. This is different from the ferromagnetic case, where $\dot{\vartheta} = 0$ for $\alpha \to 0$. However, in AFMs the tilting vanishes exactly at the resonance frequency and the tilting velocity is the highest for $\omega = \omega_n \pm \alpha/\eta$.

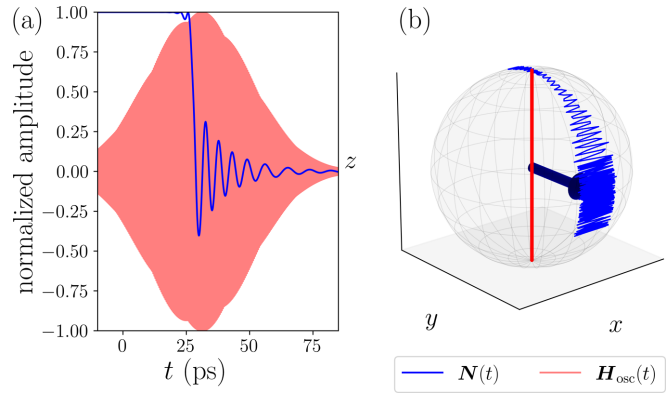

FIG. 7. 90° switching of the order parameter $\boldsymbol{N}$ using a linearly polarized field along the z axis. The material parameters are $\alpha = 0.01$, $\eta = 10$ fs, $M_0 = 2\mu_B$, and a cubic anisotropy with $K_4 = 10^{-24}$ J. The magnetic field strength is $\mu_0 h = 5$ T, the field frequency is $\omega = 1 \times 10^{14}$ s^{-1}, and the pulse width is $\sigma = 20$ ps.

Next we use atomistic spin simulations to confirm the analytical prediction that 90° switching with linearly polarized fields is possible. This switching mode is especially important in AFMs, as it can be detected by, e.g., anisotropic magnetoresistance, while a 180° reorientation of the order parameter cannot be observed experimentally. We consider a system consisting of $4 \times 4 \times 4$ antiferromagnetically coupled spins in a simple cubic arrangement with free boundary conditions. Furthermore, there is cubic anisotropy described by the Hamiltonian $\mathcal{H}_{\rm ani} = -K_4(M_{Ax}^4 + M_{Bx}^4 + M_{Ay}^4 + M_{By}^4 + M_{Az}^4 + M_{Bz}^4)/M_0^4$. At $t = 0$ ps, the order parameter points along the z direction. We apply a linearly polarized field below the nutation frequency ω_n along the z direction.

Figure 7 shows that 90° switching in AFMs is possible using a linearly polarized field. The pulse width $\sigma = 20$ ps in this simulation is identical to the value 20 ps used in the FM case. However, the switching time, i.e., the time required for the z component of the order parameter to reach $1/e$ of its initial value, is only 5 ps instead of 23 ps. Similarly to FMs, it takes a long time until the nutation is excited, as the order parameter is close to an equilibrium orientation. Applying an oscillating field slightly tilted from the equilibrium direction might significantly increase the speed of nutational switching.

Figure 8 shows that the switching time is reduced in AFMs compared to FMs for all values of inertial parameter η, external field strength h, and damping α examined. The differences are especially pronounced for low values of η, weak magnetic fields h, and small values of α. Figure 8(a) shows that for low values of η, the switching time diverges at different rates for AFMs and FMs. For AFMs, 90° switching is possible in around 10 ps for η between 10 and 100 fs. In contrast, in FMs, 90° switching can only be observed in under 30 ps for η around several hundred femtoseconds. For large values of η, the switching time in AFMs and FMs is similar. Figure 8(b) shows that nutational switching within a few tens of picoseconds requires field strengths of several tesla in both AFMs and FMs. The lower switching time in AFMs compared to FMs is more pronounced for small field strengths, while in strong magnetic fields, the switching time

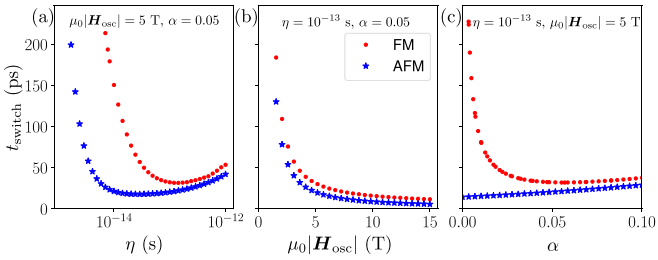

FIG. 8. Comparison of the switching times $t_{\rm switch}$ in FMs and AFMs. Shown is the time needed for the magnetization M_z or staggered magnetization N_z to decay to $1/e$ of its initial value. We consider a system without anisotropy or constant external field. The exchange constant is $J_{\rm FM} = -J_{\rm AFM} = 1.602 \times 10^{-22}$ J. For the FM the field frequency is set to $\omega = 1/\eta$, while for the AFM it is set to $\omega = \sqrt{1 + 2\gamma J\eta/M_0}/\eta - \frac{\alpha}{\eta}$.

becomes similar. Low values of α lead to diverging switching times in FMs but not in AFMs, see Fig. 8(c). For FMs this is not surprising, because the tilting velocity $\dot{\vartheta}$ is proportional to α for resonance according to Eq. (7). Since the limit of low η, h and α is relevant for the experimental realization, observing nutational switching might be more viable in AFM materials.

C. Circularly polarized fields

Next we investigate the response of the order parameter $\boldsymbol{N}$ to a circularly polarized magnetic field applied in the xy plane. We substitute the magnetic field $\boldsymbol{H}_{\rm osc} = h[\cos(\omega t)\,\hat{\mathbf{e}}_x + \sin(\omega t)\,\hat{\mathbf{e}}_y]$ in Eqs. (14) and (15) and take the time average over one nutation period. This results in

$$\ddot{\boldsymbol{N}} \cdot \hat{\mathbf{e}}_\vartheta = -\frac{(\gamma\mu_0 h)^2}{4} \frac{(\omega_{\rm n} - \omega)\omega}{(\omega_{\rm n} - \omega)^2 + \frac{\alpha^2}{\eta^2}} \sin(2\vartheta), \tag{17}$$

$$\ddot{\boldsymbol{N}} \cdot \hat{\mathbf{e}}_\varphi = (\gamma\mu_0 h)^2 \frac{\frac{\alpha}{\eta}\omega}{(\omega_{\rm n} - \omega)^2 + \frac{\alpha^2}{\eta^2}} \sin(\vartheta). \tag{18}$$

An illustration of the right-hand side of Eq. (17) is shown in Fig. 9(a). Again, different from the FM case, the sign of $\ddot{\boldsymbol{N}} \cdot \hat{\mathbf{e}}_\vartheta$ in Eq. (17) depends on the external field frequency ω. For a frequency lower than the nutation frequency $\omega < \omega_{\rm n}$, the order parameter is stable if it is perpendicular to the external

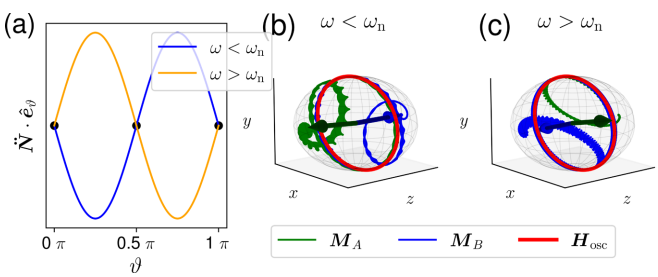

FIG. 9. Illustration of the nutational switching mode in AFMs for a circularly polarized field. (a) The right-hand side of Eq. (17) as a function of ϑ. (b, c) Illustration of the switching modes when applying a circularly polarized magnetic field to AFMs for frequencies ω (b) below and (c) above the nutation frequency $\omega_{\rm n}$.

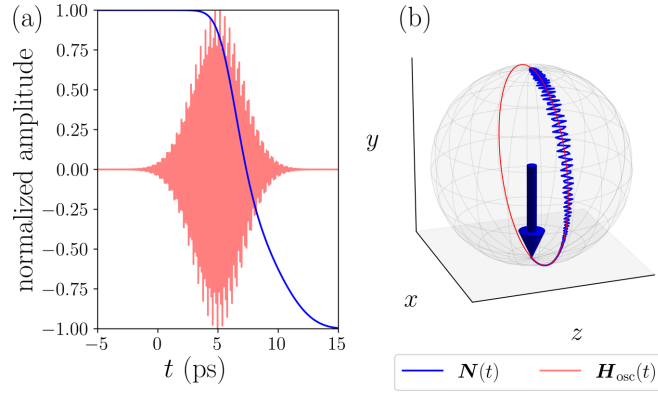

FIG. 10. 180° switching of the order parameter $\boldsymbol{N}$ using a circularly polarized field in the xy plane. The material parameters are $\alpha = 0.05$, $\eta = 10$ fs, $M_0 = 2\mu_{\rm B}$, $J = 1.602 \times 10^{-22}$ J $= 1$ meV and a uniaxial anisotropy along the y axis with $K_y = 10^{-24}$ J. The magnetic field strength is $\mu_0 h = 5$ T, the field frequency is $\omega = 1.1 \times 10^{14}$ s^{-1}, and the pulse width is $\sigma = 2$ ps.

field at $\vartheta = 0$ or $\vartheta = \pi$, and unstable if it is in the plane of the field at $\vartheta = \pi/2$. For all other orientations, the order parameter will align itself perpendicular to the external field, similarly to the FM case. This switching mode is shown in Fig. 9(b). For frequencies higher than the nutation frequency $\omega > \omega_{\rm n}$, the order parameter is stable if it is in the plane of the external field and unstable if it is perpendicular to the magnetic field. Therefore the order parameter aligns itself in the plane of the external field, where it rotates according to Eq. (18). This can be used for 180° switching, as illustrated in Fig. 9(c).

Again, in contrast to FMs, in AFMs we find two possible switching modes: from the plane of the excitation towards the perpendicular direction, or the other way around, depending on the excitation frequency. These switching modes are also visualized in Supplemental Video 4 [26]. This is a consequence of the AFM coupling. In a FM, a state can only be stationary if the torque exerted by the external field vanishes. In AFMs a state can also be stationary if the torques exerted on the two sublattices cancel each other. This is the case for $\vartheta = \pi/2$. Another difference from the FM case is that $\vartheta = 0$ and π always have the same stability, instead of one configuration being favored depending on the sense of rotation of the external field. This can be explained by the sublattice symmetry of AFMs. Since the sublattices are identical, the order parameter has to behave the same way if its direction is inverted. Equation (18) shows that the order parameter rotates around the z axis, similarly to the angular momentum in the single-spin case in Eq. (9). The rotation vanishes if the order parameter is parallel or antiparallel to the external field.

We also examine the behavior of the order parameter using atomistic spin simulations. Analogously to the FM case, we use circularly polarized pulses for 180° switching along the y axis. We consider a system with uniaxial anisotropy along the y axis, $\mathcal{H}_{\rm ani} = -\frac{K_y}{M_0^2}(M_{Ay}^2 + M_{By}^2)$. At $t = 0$ s, the order parameter is parallel to the y direction.

Figure 10 shows that 180° switching is possible using circularly polarized fields. Compared to FMs, significantly

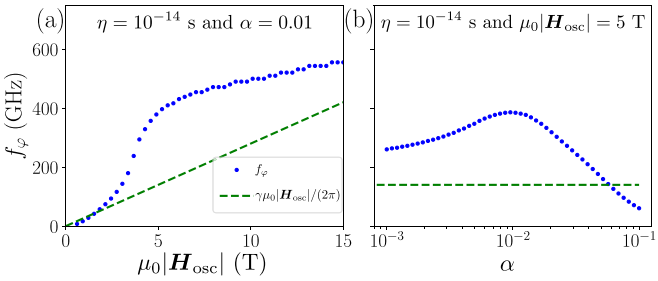

FIG. 11. Comparison between precession frequency $\gamma\mu_0|\boldsymbol{H}_{\rm osc}|/(2\pi)$ and nutation-driven 180° switching frequency f_φ. The material parameters are as in Fig. 10 but with zero anisotropy. A circularly polarized field is continuously applied in the xy plane with $\omega = 1.12 \times 10^{14}$ s^{-1}. f_φ is calculated for a rotation around the z axis over the first half period.

lower pulse widths are sufficient, $\sigma = 2$ ps instead of $\sigma = 10$ ps in Fig. 5. Moreover, the switching itself is possible within 5 ps. This is a significant advantage, as the switching process is faster. Another advantage is that in this case the order parameter always remains parallel to the plane of the magnetic field. Therefore the switching mode can fully invert the spin without relying on relaxation. Nevertheless, the anisotropy energy is an order of magnitude lower than in the FM example in Fig. 5. Atomistic spin simulations indicate that nutational switching in AFMs is only possible for very weak anisotropy.

For a continuously applied ac magnetic field, the order parameter continuously rotates in the xy plane with frequency $f_\varphi = \dot{\varphi}/(2\pi)$. To investigate how this frequency varies for different material parameters, we will neglect the uniaxial anisotropy, since otherwise the rotation frequency is not a constant but varies with the angle ϑ. Figure 11(a) shows that the switching frequency increases with increasing magnetic field, as Eq. (18) implies. Note that Eq. (18) does not give the rotation frequency directly. Therefore we can expect only qualitative agreement and not quantitatively the same relationship. For field strengths of several tesla, the switching frequency f_φ significantly exceeds the precession frequency $\omega_{\rm p} = \gamma h$ at comparable magnetic fields. The reason for this is that the resonant excitation of the nutation induces a torque proportional to h^2, while the velocity of precessional switching is proportional to h. A field strength of 5 T switches the spin in approximately 2.5 ps. Using higher field strengths than 5 T provides only diminishing returns, since deviations from the linear-response relation $f_\varphi \propto h^2$ may be observed in this regime. Switching is also possible for lower field strengths but is significantly slower. The simulations indicate that for field strengths lower than 1 T, switching becomes impossible.

Figure 11(b) shows that the switching speed is highest for $\alpha = 0.01$. For very low values of α the switching frequency is diminished but is still significantly higher than for precessional switching. For a value of α greater than 0.01, the switching frequency drops significantly as the nutation becomes suppressed. Therefore, nutational switching can most likely be observed in the low-damping regime.

V. CONCLUSION

Using analytic methods and numerical spin simulations of the ILLG equation, we explored nutation-driven switching using oscillating magnetic fields. Analytically, we demonstrated that a sinusoidal magnetic field excites a nutational motion of the magnetic moment around the angular momentum, with a resonant enhancement at the nutation frequency. The nutation in conjunction with the oscillating field exerts a torque on the angular momentum.

This torque can drive either 90° or 180° nutational switching, depending on the polarization and the frequency of the field. A linearly polarized magnetic field applied to a FM aligns the angular momentum perpendicular to the field. Using numerical spin simulations, we demonstrated that this enables 90° switching using Gaussian pulses for materials with cubic anisotropy. A circularly polarized field in the xy plane aligns the angular momentum along the z direction. The angular momentum continuously rotates in the xy plane, enabling 180° switching for Gaussian pulses.

Nutational switching in AFMs is overall similar to FMs for external field frequencies below the nutation frequency, but it proceeds faster because of the intrinsic inertia caused by the exchange interaction between the sublattices. However, for frequencies above the nutation frequency, the order parameter aligns itself parallel to the external field. For circularly polarized fields, this means that the order parameter rotates in the plane of the external field with high frequency. The rotation frequency $\dot{\varphi} \propto h^2$ increases faster than the precession frequency $\omega_{\rm p} = \gamma h$, enabling faster switching than using precession-based methods. Nutational switching in AFMs is favored in materials with low damping and low anisotropy.

Using realistic parameter values, we found that a sufficiently fast nutational switching can be observed for oscillating magnetic fields with an amplitude of $\mu_0 h = 5$ T, the technology for achieving which is likely not available at the present moment. However, by choosing the right material the required field strengths might be significantly lowered. As nutational switching is tied to the nutation amplitude, materials with large values of η can reduce the required magnetic fields. Furthermore, switching is possible at lower magnetic fields than 5 T, even though it is significantly slower. An interesting possibility for further studies is generating a large nutation amplitude with a dc magnetic field pulse. The nutation energy might then be used for switching using a significantly weaker terahertz ac magnetic field. Constant field pulses can be generated using linear accelerators. More accessible methods for this in the future include magnetic-field-enhancing metamaterials [28], vector laser beams [29], or ultrafast electronic switches [30]. In the future, nutation might be used for faster and more energy-efficient switching of the magnetic state, as the energy stored in the nutation can be extracted during the switching.

ACKNOWLEDGMENTS

The authors would like to thank Ritwik Mondal and Mikhail Cherkasskii for fruitful discussions. Financial support by the German Research Foundation via SFB 1432, by

the National Research, Development and Innovation Office of Hungary via Project No. K131938 and by the Young Scholar Fund at the University of Konstanz is gratefully acknowledged.

APPENDIX A: REPRESENTING THE ILLG EQUATION USING THE ANGULAR MOMENTUM

In this section we express the ILLG equation (1) using the angular momentum $\boldsymbol{L}_i$. The angular momentum is given by [5]

$$\boldsymbol{L}_i = \frac{1}{\gamma_i}\boldsymbol{M}_i - \frac{\eta_i}{M_{0,i}\gamma_i}\boldsymbol{M}_i \times \dot{\boldsymbol{M}}_i = \frac{1}{\gamma_i}\boldsymbol{M}_i - \Delta\boldsymbol{L}_i, \tag{A1}$$

if an inertial term is considered.

The time derivative of the angular momentum is then described as

$$\dot{\boldsymbol{L}}_i = \frac{1}{\gamma_i}\dot{\boldsymbol{M}}_i - \frac{\eta_i}{M_{0,i}\gamma}\boldsymbol{M}_i \times \ddot{\boldsymbol{M}}_i. \tag{A2}$$

Next we eliminate $\ddot{\boldsymbol{M}}_i$ from Eq. (A2) using the ILLG equation (1). This results in

$$\begin{aligned}\gamma_i\dot{\boldsymbol{L}}_i &= \gamma_i\left(\frac{1}{\gamma_i}\dot{\boldsymbol{M}}_i - \frac{\eta_i}{M_{0,i}\gamma_i}\boldsymbol{M}_i \times \ddot{\boldsymbol{M}}_i\right)\\ &= -\gamma_i\boldsymbol{M}_i \times \mu_0\boldsymbol{H}_{\mathrm{eff},i} + \frac{\alpha_i}{M_{0,i}}\boldsymbol{M}_i \times \dot{\boldsymbol{M}}_i.\end{aligned} \tag{A3}$$

Equation (A3) describes that the time evolution of the angular momentum is driven by a precessional torque and a damping term.

By using the fact that $\boldsymbol{M}_i \times \dot{\boldsymbol{M}}_i = \frac{\gamma_i M_{0,i}}{\eta_i}(\frac{1}{\gamma_i}\boldsymbol{M}_i - \boldsymbol{L}_i)$ according to Eq. (A1), we obtain

$$\dot{\boldsymbol{L}}_i = -\boldsymbol{M}_i \times \mu_0\boldsymbol{H}_{\mathrm{eff},i} + \frac{\alpha_i}{\gamma_i\eta_i}\boldsymbol{M}_i - \frac{\alpha_i}{\eta_i}\boldsymbol{L}_i. \tag{A4}$$

Therefore we found a first-order explicit differential equation for $\boldsymbol{L}_i$. Next we express $\dot{\boldsymbol{M}}_i$ from Eq. (A1). This can be done by multiplying the equation by $\boldsymbol{M}_i\times$ and using the triple vector product

$$\begin{aligned}\boldsymbol{M}_i \times \boldsymbol{L}_i = &-\frac{\eta_i}{\gamma_i M_{0,i}}(\underbrace{(\boldsymbol{M}_i \cdot \dot{\boldsymbol{M}}_i)}_{=0}\boldsymbol{M}_i\\ &- \underbrace{(\boldsymbol{M}_i \cdot \boldsymbol{M}_i)}_{=M_{0,i}^2}\dot{\boldsymbol{M}}_i) = \frac{\eta_i M_{0,i}}{\gamma_i}\dot{\boldsymbol{M}}_i.\end{aligned} \tag{A5}$$

Here we used that the ILLG equation conserves the length of the magnetic moment, meaning that $\boldsymbol{M}_i$ and $\dot{\boldsymbol{M}}_i$ are perpendicular to each other. The new equations of motion can be written as

$$\dot{\boldsymbol{L}}_i = -\boldsymbol{M}_i \times \mu_0\boldsymbol{H}_{\mathrm{eff},i} + \frac{\alpha_i}{\eta_i}\left(\frac{1}{\gamma_i}\boldsymbol{M}_i - \boldsymbol{L}_i\right), \tag{A6}$$

$$\dot{\boldsymbol{M}}_i = \frac{\gamma_i}{\eta_i M_{0,i}}\boldsymbol{M}_i \times \boldsymbol{L}_i. \tag{A7}$$

According to Eq. (A1), we can write $\boldsymbol{M}_i$ as $\boldsymbol{M}_i = \gamma_i(\boldsymbol{L}_i + \Delta\boldsymbol{L}_i)$. By substituting this into Eq. (A7) we obtain

$$\dot{\boldsymbol{L}}_i + \Delta\dot{\boldsymbol{L}}_i = \frac{\gamma_i}{\eta_i M_{0,i}}\Delta\boldsymbol{L}_i \times \boldsymbol{L}_i. \tag{A8}$$

Now we can use Eq. (A6) to eliminate $\dot{\boldsymbol{L}}_i$, resulting in Eqs. (3) and (4) in the main text.

APPENDIX B: DIFFERENTIAL EQUATION FOR THE NUTATION VECTOR

We will assume that the system is originally in equilibrium, where $\boldsymbol{L}_i$ and $\boldsymbol{M}_i$ are parallel. The nutation is excited by the oscillating external field, which is assumed to be small in order to remain in the linear-response regime. While the length of $\boldsymbol{M}_i$ is conserved in Eq. (1), in the limit of low nutation amplitude it can also be assumed that the magnitude of $\boldsymbol{L}_i$ is conserved on the timescale of the order of the nutation period. We set $\boldsymbol{L}_i = L_{0,i}\hat{\mathbf{e}}_{r,i}$, and we assume $\Delta\boldsymbol{L}_i = a_i(t)\hat{\mathbf{e}}_{\vartheta,i} + b_i(t)\hat{\mathbf{e}}_{\varphi,i}$. The assumption that the nutation is in the plane perpendicular to $\boldsymbol{L}_i$ is justified for a small nutation amplitude, because $\boldsymbol{L}_i \cdot \Delta\boldsymbol{L}_i = -|\Delta\boldsymbol{L}_i|^2 \approx 0$. We substitute the approximation for $\Delta\boldsymbol{L}_i$ into Eq. (4). Furthermore, we assume that the time derivatives of the basis vectors $\hat{\mathbf{e}}_{r,i}$, $\hat{\mathbf{e}}_{\varphi,i}$, and $\hat{\mathbf{e}}_{\vartheta,i}$ can be neglected on the fast timescale on which the nutation takes place. This results in

$$\begin{aligned}\dot{a}_i\hat{\mathbf{e}}_{\vartheta,i} + \dot{b}_i\hat{\mathbf{e}}_{\varphi,i} = &\frac{M_{0,i}}{\eta_i}(-a_i\hat{\mathbf{e}}_{\varphi,i} + b_i\hat{\mathbf{e}}_{\vartheta,i})\\ &+ M_{0,i}\hat{\mathbf{e}}_{r,i} \times \mu_0\boldsymbol{H}_{\mathrm{eff},i} + \gamma_i(a_i\hat{\mathbf{e}}_{\vartheta,i} \times \mu_0\boldsymbol{H}_{\mathrm{eff},i}\\ &+ b_i\hat{\mathbf{e}}_{\varphi,i} \times \mu_0\boldsymbol{H}_{\mathrm{eff},i}) - \frac{\alpha_i}{\eta_i}(a_i\hat{\mathbf{e}}_{\vartheta,i} + b_i\hat{\mathbf{e}}_{\varphi,i}).\end{aligned} \tag{B1}$$

By projecting on the $\hat{\mathbf{e}}_{\vartheta,i}$ and $\hat{\mathbf{e}}_{\varphi,i}$ directions we obtain

$$\begin{aligned}\dot{a}_i = &-\frac{\alpha_i}{\eta_i}a_i + \frac{L_{0,i}\gamma_i}{M_{0,i}\eta_i}b_i + \gamma_i b_i\mu_0\boldsymbol{H}_{\mathrm{eff},i} \cdot \hat{\mathbf{e}}_{r,i}\\ &- M_{0,i}\hat{\mathbf{e}}_{\varphi,i} \cdot \mu_0\boldsymbol{H}_{\mathrm{eff},i},\end{aligned} \tag{B2}$$

$$\begin{aligned}\dot{b}_i = &-\frac{\alpha_i}{\eta_i}b_i - \frac{L_{0,i}\gamma_i}{M_{0,i}\eta_i}a_i - \gamma_i a_i\mu_0\boldsymbol{H}_{\mathrm{eff},i} \cdot \hat{\mathbf{e}}_{r,i}\\ &+ M_{0,i}\hat{\mathbf{e}}_{\vartheta,i} \cdot \mu_0\boldsymbol{H}_{\mathrm{eff},i}.\end{aligned} \tag{B3}$$

To express $L_{0,i}$, we use the approximation

$$\begin{aligned}L_{0,i}^2 = \left|\frac{1}{\gamma_i}\boldsymbol{M}_i - \frac{\eta_i}{M_{0,i}\gamma_i}\boldsymbol{M}_i \times \dot{\boldsymbol{M}}_i\right|^2 &= \frac{1}{\gamma_i^2}|\boldsymbol{M}_i|^2 + \frac{\eta_i^2}{\gamma_i^2}|\dot{\boldsymbol{M}}_i|^2\\ \approx \frac{1}{\gamma_i^2}|\boldsymbol{M}_i|^2 &= \frac{M_{0,i}^2}{\gamma_i^2}.\end{aligned} \tag{B4}$$

Here we used the fact that $\boldsymbol{M}_i \cdot (\boldsymbol{M}_i \times \dot{\boldsymbol{M}}_i) = 0$ and $\boldsymbol{M}_i \perp \dot{\boldsymbol{M}}_i$. This approximation becomes exact for vanishing nutation amplitude. Using this we obtain $\frac{L_{0,i}\gamma_i}{M_{0,i}\eta_i} \approx \frac{1}{\eta_i}$. Next we combine Eqs. (B2) and (B3) into

$$\begin{aligned}\partial_t(a_i + ib_i) = &-\frac{\alpha_i}{\eta_i}(a_i + ib_i) - \frac{L_{0,i}\gamma_i}{M_{0,i}\eta_i}(ia_i - b_i)\\ &- \gamma_i(ia_i - b_i)\mu_0\boldsymbol{H}_{\mathrm{eff},i} \cdot \hat{\mathbf{e}}_{r,i}\\ &- M_{0,i}(\hat{\mathbf{e}}_{\varphi,i} - i\hat{\mathbf{e}}_{\vartheta,i}) \cdot \mu_0\boldsymbol{H}_{\mathrm{eff},i}.\end{aligned} \tag{B5}$$

By defining $c_i(t) = a_i(t) + ib_i(t)$, this simplifies to

$$\begin{aligned}\dot{c}_i = &-i\omega_{\mathrm{n},i}c_i(t) - \frac{\alpha_i}{\eta_i}c_i(t)\\ &- M_{0,i}(\hat{\mathbf{e}}_{\varphi,i} - i\hat{\mathbf{e}}_{\vartheta,i}) \cdot \mu_0\boldsymbol{H}_{\mathrm{eff},i},\end{aligned} \tag{B6}$$

with $\omega_{\mathrm{n},i} = \frac{1}{\eta_i} + \gamma_i\mu_0\boldsymbol{H}_{\mathrm{eff},i} \cdot \hat{\mathbf{e}}_r$ the nutation frequency.

Next we will solve Eq. (B6) for a single macrospin describing a ferromagnetic particle. As there is only one sublattice, we drop the index i. Assuming that $\boldsymbol{H}_{\text{eff}}$ does not depend on the nutation amplitude $c(t)$, a closed-form solution can be calculated. The solution to the homogeneous part is given by

$$c_{\text{hom}}(t) = c_0 e^{-\frac{\alpha}{\eta}t} e^{-i\int_0^t \omega_{\text{n}}(t')dt'}. \tag{B7}$$

The nutation is a circular motion with exponentially decaying amplitude.

In the presence of an effective field $\boldsymbol{H}_{\text{eff}}$, the solution to the inhomogeneous equation is given by

$$c(t) = c_{\text{hom}}(t)\left(1 - M_0 \int_0^t dt' c_{\text{hom}}^{-1}(t')\,(\hat{\mathbf{e}}_\varphi - i\hat{\mathbf{e}}_\vartheta)\cdot\mu_0\boldsymbol{H}_{\text{eff}}(t')\right). \tag{B8}$$

In the main text we rewrote Eq. (B8) in the form of Eq. (5) for analyzing the nutation amplitude in the presence of anisotropy, a static field, and an oscillating field.

APPENDIX C: CONNECTION BETWEEN DAMPING AND NUTATION

For a system with an oscillating field, uniaxial anisotropy, and a static field, we can explicitly evaluate the damping term $\langle\frac{\alpha}{\eta}\Delta\boldsymbol{L}\rangle_t$ in Eq. (6). For this purpose we use the closed-form solution for the nutation, Eq. (B8). By using $\omega_{\text{n}} \approx \frac{1}{\eta}$ and $\langle\boldsymbol{H}_{\text{eff}}\rangle_t = \langle\boldsymbol{H}_{\text{osc}}(t) + \boldsymbol{H}_0\rangle_t = \boldsymbol{H}_0$, we arrive at

$$\left\langle\frac{\alpha}{\eta}\Delta\boldsymbol{L}\right\rangle_t = M_0\mu_0\frac{\alpha}{1+\alpha^2}[(\hat{\mathbf{e}}_\vartheta\cdot\boldsymbol{H}_0)\hat{\mathbf{e}}_\vartheta + (\hat{\mathbf{e}}_\varphi\cdot\boldsymbol{H}_0)\hat{\mathbf{e}}_\varphi + \alpha[(\hat{\mathbf{e}}_\vartheta\cdot\boldsymbol{H}_0)\hat{\mathbf{e}}_\varphi - (\hat{\mathbf{e}}_\varphi\cdot\boldsymbol{H}_0)\hat{\mathbf{e}}_\vartheta]]. \tag{C1}$$

The first two terms describe the same damping process as in the LLG equation. The angular momentum will align itself parallel to the magnetic field $\boldsymbol{H}_0$. The speed of the relaxation is controlled by the parameter α. Note that Eq. (C1) does not explicitly depend on η, demonstrating that there are no inertial effects in this case. The third and fourth terms on the right-hand side of Eq. (C1) describe a damping-related modification to the precession frequency.

APPENDIX D: NUTATION IN ANTIFERROMAGNETS

We express the angular momenta of the sublattices in spherical coordinates $\boldsymbol{L}_A = L_0\hat{\mathbf{e}}_{r,A}$ and $\boldsymbol{L}_B = L_0\hat{\mathbf{e}}_{r,B}$. In AFMs, the total magnetization is minimized by the AFM coupling, $\boldsymbol{M} = \boldsymbol{M}_A + \boldsymbol{M}_B \approx 0$. Therefore the angular momenta of the two sublattices must be approximately antiparallel, $\boldsymbol{L}_A \approx -\boldsymbol{L}_B$. This enables us to express the orientation of the sublattices in terms of two global angles $\vartheta = \vartheta_A$ and $\varphi = \varphi_A$. These angles define the orientation of the order parameter $\boldsymbol{N} = \boldsymbol{M}_A - \boldsymbol{M}_B$. For the basis vectors this means $\hat{\boldsymbol{e}}_{r,A} = -\hat{\boldsymbol{e}}_{r,B}$, $\hat{\boldsymbol{e}}_{\vartheta,A} = \hat{\boldsymbol{e}}_{\vartheta,B}$, and $\hat{\boldsymbol{e}}_{\varphi,A} = -\hat{\boldsymbol{e}}_{\varphi,B}$. Here the perpendicular component of the effective field $(\hat{\mathbf{e}}_{\varphi,i} - i\hat{\mathbf{e}}_{\vartheta,i})\cdot\mu_0\boldsymbol{H}_{\text{eff},i}$ in Eq. (B6) contains terms which are linear in c_A and c_B because of the AFM exchange interaction. This leads to the following system of differential equations:

$$\dot{c}_A = -i\omega_A c_A - \frac{\alpha}{\eta}c_A - i\gamma^2 L_0 J c_B^* + f_A(t), \tag{D1}$$

$$\dot{c}_B^* = -i\omega_B c_B^* - \frac{\alpha}{\eta}c_B^* + i\gamma^2 L_0 J c_A + f_B^*(t), \tag{D2}$$

with $\omega_{A/B} = \gamma\mu_0\boldsymbol{H}_{\text{ext}}\cdot\hat{\mathbf{e}}_r \pm (\frac{1}{\eta} - \gamma\mu_0\boldsymbol{H}_{\text{ani},A/B}\cdot\hat{\mathbf{e}}_r + \gamma^2 L_0\frac{J}{M_0^2})$ and $f_{A/B} = M_0\mu_0(\hat{\mathbf{e}}_\varphi \mp i\hat{\mathbf{e}}_\vartheta)\cdot(\boldsymbol{H}_{\text{ext}} + \boldsymbol{H}_{\text{ani},A/B})$.

The homogeneous solution to this system of differential equations can be obtained by diagonalizing the corresponding dynamical matrix, yielding

$$\begin{pmatrix} c_A \\ c_B^* \end{pmatrix} = \begin{pmatrix} \sigma_A \\ 1 \end{pmatrix} e^{-i\omega_{\text{n},A}t} e^{-\frac{\alpha}{\eta}t} + \begin{pmatrix} \sigma_B \\ 1 \end{pmatrix} e^{i\omega_{\text{n},B}t} e^{-\frac{\alpha}{\eta}t}, \tag{D3}$$

with $A = [M_0 - 2K(\boldsymbol{u}\cdot\hat{\mathbf{e}}_r)^2\eta\gamma]\cdot[M_0 + 2J\eta\gamma - 2K(\boldsymbol{u}\cdot\hat{\mathbf{e}}_r)^2\eta\gamma]$, $\omega_{\text{n},A/B} = (\frac{\sqrt{A}}{M_0\eta} \pm \gamma\hat{\mathbf{e}}_r\cdot\mu_0\boldsymbol{H}_0)$, $\sigma_B = \frac{M_0 + J\eta\gamma - 2K\eta\gamma(\hat{\mathbf{e}}_r\cdot\boldsymbol{u})^2 - \sqrt{A}}{J\eta\gamma}$, and $\sigma_A = \sigma_B + 2\frac{\sqrt{A}}{J\eta\gamma}$:

$$\begin{aligned} c_A = \mu_0 M_0 \frac{(\hat{\mathbf{e}}_\varphi - i\hat{\mathbf{e}}_\vartheta)}{\sigma_A - \sigma_B}\cdot\Bigg[&\frac{\sigma_B \boldsymbol{h} e^{-i\omega t}}{i(\omega_{\text{n},B} - \omega) + \frac{\alpha}{\eta}} + \frac{\sigma_A\sigma_B \boldsymbol{h}^* e^{i\omega t}}{i(\omega_{\text{n},B} + \omega) + \frac{\alpha}{\eta}} - \frac{\sigma_A \boldsymbol{h} e^{-i\omega t}}{-i(\omega_{\text{n},A} + \omega) + \frac{\alpha}{\eta}} \\ &- \frac{\sigma_A\sigma_B \boldsymbol{h}^* e^{i\omega t}}{-i(\omega_{\text{n},A} - \omega) + \frac{\alpha}{\eta}}\Bigg], \end{aligned} \tag{D4}$$

$$\begin{aligned} c_B = M_0\mu_0 \frac{(\hat{\mathbf{e}}_\varphi + i\hat{\mathbf{e}}_\vartheta)}{\sigma_A - \sigma_B}\cdot\Bigg[&\frac{\boldsymbol{h}^* e^{i\omega t}}{-i(\omega_{\text{n},B} - \omega) + \frac{\alpha}{\eta}} + \frac{\sigma_A \boldsymbol{h} e^{-i\omega t}}{-i(\omega_{\text{n},B} + \omega) + \frac{\alpha}{\eta}} \\ &- \frac{\boldsymbol{h}^* e^{i\omega t}}{i(\omega_{\text{n},A} + \omega) + \frac{\alpha}{\eta}} - \frac{\sigma_B \boldsymbol{h} e^{-i\omega t}}{i(\omega_{\text{n},A} - \omega) + \frac{\alpha}{\eta}}\Bigg]. \end{aligned} \tag{D5}$$

Discussing nutational switching based on the above equation is rather convoluted. Therefore we will only consider the case where $\omega_{\text{n},A} \approx \omega_{\text{n},B} \approx \frac{\sqrt{A}}{M_0\eta}$, which is usually the case, as the nutation frequency $\frac{\sqrt{A}}{M_0\eta}$ is much greater than the precession frequency $\gamma|\boldsymbol{H}_0|$. Moreover, for $\sigma_A \to 0$ the nutation modes of the sublattices Eq. (D3) decouple. Following a Taylor expansion of $\sqrt{A}$ in $J\eta\gamma$ up to the second order, we find $\sigma_A = \frac{J\eta\gamma}{2[M_0 - 2K\eta\gamma(\hat{e}_r\cdot\boldsymbol{u})^2]}$. If the anisotropy is weak, the sublattices decouple under the condition $J \ll 2\frac{M_0}{\eta\gamma}$. In the simulations we considered, $\eta = 10$ fs and $M_0 = 2\mu_{\text{B}}$, requiring $J \ll 1.055 \times 10^{-20}$ J. For the value of $J = 1.602 \times 10^{-22}$ $J = 1$ meV, this approximation is well justified. In this case, Eqs. (D4) and (D5) have the same form as the single-spin nutation solution Eq. (5).

APPENDIX E: ORDER PARAMETER IN AFMS

In this section we derive the differential equation (12) for the order parameter $\boldsymbol{N}$ in AFMs. The derivation is similar to a previous work by Gomonaĭ *et al.* [31] without the inertial term. We add $\Delta\dot{\boldsymbol{L}}_{A/B}$ to Eq. (3) and multiply by $\gamma_{A/B} = \gamma$.

This results in the following differential equations for the magnetizations $\boldsymbol{M}_{A/B}$ of the different sublattices:

$$\dot{\boldsymbol{M}}_A = -\gamma \boldsymbol{M}_A \times \mu_0 \boldsymbol{H}_A + \frac{\gamma J}{M_0^2} \boldsymbol{M}_A \times \boldsymbol{M}_B + \left(\partial_t + \frac{\alpha}{\eta}\right) \gamma \Delta \boldsymbol{L}_A, \tag{E1}$$

$$\dot{\boldsymbol{M}}_B = -\gamma \boldsymbol{M}_B \times \mu_0 \boldsymbol{H}_B + \frac{\gamma J}{M_0^2} \boldsymbol{M}_B \times \boldsymbol{M}_A + \left(\partial_t + \frac{\alpha}{\eta}\right) \gamma \Delta \boldsymbol{L}_B, \tag{E2}$$

with $\boldsymbol{H}_{A/B} = \boldsymbol{H}_{\text{ext}} + \boldsymbol{H}_{\text{ani},A/B}$. Next we define the magnetization $\boldsymbol{M} = \boldsymbol{M}_A + \boldsymbol{M}_B$ and the staggered magnetization $\boldsymbol{N} = \boldsymbol{M}_A - \boldsymbol{M}_B$. The effective fields for the magnetization and staggered magnetization are given by $\boldsymbol{H}_M = (\boldsymbol{H}_A + \boldsymbol{H}_B)/2$ and $\boldsymbol{H}_N = (\boldsymbol{H}_A - \boldsymbol{H}_B)/2$. By summing up and subtracting Eqs. (E1) and (E2), we find a system of differential equations for $\boldsymbol{M}$ and $\boldsymbol{N}$:

$$\dot{\boldsymbol{M}} = -\gamma(\boldsymbol{M} \times \boldsymbol{H}_M + \boldsymbol{N} \times \mu_0 \boldsymbol{H}_N) + \boldsymbol{T}_M, \tag{E3}$$

$$\dot{\boldsymbol{N}} = -\gamma(\boldsymbol{N} \times \mu_0 \boldsymbol{H}_M + \boldsymbol{M} \times \mu_0 \boldsymbol{H}_N) + \frac{\gamma J}{M_0^2} \boldsymbol{N} \times \boldsymbol{M} + \boldsymbol{T}_N, \tag{E4}$$

with $\boldsymbol{T}_M = (\partial_t + \frac{\alpha}{\eta})(\Delta \boldsymbol{L}_A + \Delta \boldsymbol{L}_B)$ and $\boldsymbol{T}_N = (\partial_t + \frac{\alpha}{\eta})(\Delta \boldsymbol{L}_A - \Delta \boldsymbol{L}_B)$.

By multiplying Eq. (E4) with $\boldsymbol{N}\times$ and applying the triple vector product, we can find an explicit expression for $\boldsymbol{M}$. Using the fact that for antiferromagnets $\boldsymbol{M} \cdot \boldsymbol{N} = 0$, and the approximation that the anisotropy is much smaller than the exchange interaction, we find the expression

$$\boldsymbol{M} \approx -\frac{4}{\gamma J}(\boldsymbol{N} \times \dot{\boldsymbol{N}} + \gamma \boldsymbol{N} \times (\boldsymbol{N} \times \mu_0 \boldsymbol{H}_M) - \boldsymbol{N} \times \boldsymbol{T}_N). \tag{E5}$$

We can now substitute this into Eq. (E3). This reveals

$$\begin{aligned} &\boldsymbol{N} \times \ddot{\boldsymbol{N}} + \gamma \partial_t (\boldsymbol{N} \times (\boldsymbol{N} \times \mu_0 \boldsymbol{H}_M) - \boldsymbol{N} \times \boldsymbol{T}_N) \\ &\quad - \frac{\gamma^2 J}{4} \boldsymbol{N} \times \mu_0 \boldsymbol{H}_N \\ &= -\gamma (\boldsymbol{N} \times \dot{\boldsymbol{N}} + \gamma \boldsymbol{N} \times (\boldsymbol{N} \times \mu_0 \boldsymbol{H}_M) \\ &\quad - \boldsymbol{N} \times \boldsymbol{T}_N) \times \mu_0 \boldsymbol{H}_M - \frac{\gamma J}{4} \boldsymbol{T}_M. \end{aligned} \tag{E6}$$

We can now simplify $\boldsymbol{N} \times (\boldsymbol{N} \times \mu_0 \boldsymbol{H}_M) = (\boldsymbol{N} \cdot \mu_0 \boldsymbol{H}_M)\boldsymbol{N} - 4M_0^2 \mu_0 \boldsymbol{H}_M$. Therefore we obtain $[\boldsymbol{N} \times (\boldsymbol{N} \times \mu_0 \boldsymbol{H}_M)] \times \mu_0 \boldsymbol{H}_M = (\boldsymbol{N} \cdot \mu_0 \boldsymbol{H}_M)(\boldsymbol{N} \times \mu_0 \boldsymbol{H}_M)$. Moreover, using the assumption that the nutation $\Delta \boldsymbol{L}_N$ occurs in the plane perpendicular to $\boldsymbol{N}$, we obtain $\boldsymbol{N} \cdot \boldsymbol{T}_N \approx 0$ and $\boldsymbol{N} \cdot \dot{\boldsymbol{N}} \approx 0$ from Eq. (E4), i.e., the length of the staggered magnetization is conserved. This implies $\boldsymbol{N} \times (\dot{\boldsymbol{N}} \times \mu_0 \boldsymbol{H}_M) \approx (\boldsymbol{N} \mu_0 \boldsymbol{H}_M)\dot{\boldsymbol{N}}$. This simplifies Eq. (E6) to (12) in the main text.

APPENDIX F: NUTATION TERM IN ANTIFERROMAGNETS IN SPHERICAL COORDINATES

In antiferromagnets, the term $\gamma(\boldsymbol{N} \times \boldsymbol{T}_N) \times \mu_0 \boldsymbol{H}_M \approx \gamma(\boldsymbol{N} \times \partial_t \Delta \boldsymbol{L}_N) \times \mu_0 \boldsymbol{H}_M$ in Eq. (E6) is responsible for nutational switching. Here we evaluate this term using the closed-form solution for the nutation vector in Eqs. (D4) and (D5). We assume $\omega_{\text{n},A} \approx \omega_{\text{n},B} \approx \omega_{\text{n}}$, which is valid since the precession frequency is much smaller than the nutation frequency. First we know that $\Delta \boldsymbol{L}_N = \text{Re}\{c_A\}\hat{\boldsymbol{e}}_\vartheta + \text{Im}\{c_A\}\hat{\boldsymbol{e}}_\varphi - (\text{Re}\{c_B\}\hat{\boldsymbol{e}}_\vartheta - \text{Im}\{c_B\}\hat{\boldsymbol{e}}_\varphi) = \text{Re}\{c_A - c_B^*\}\hat{\boldsymbol{e}}_\vartheta + \text{Im}\{c_A - c_B^*\}\hat{\boldsymbol{e}}_\varphi$. According to Eqs. (10) and (11),

$$\begin{aligned} c_A - c_B^* = M_0 \mu_0 \Bigg\{ &\frac{-\hat{\boldsymbol{e}}_\varphi + i\hat{\boldsymbol{e}}_\vartheta}{(\omega_{\text{n}} - \omega)^2 + \frac{\alpha^2}{\eta^2}} \cdot \Bigg[i(\omega_{\text{n}} - \omega)(-\boldsymbol{h} e^{-i\omega t} \\ &+ \boldsymbol{h}^* e^{i\omega t}) + \frac{\alpha}{\eta}(\boldsymbol{h} e^{-i\omega t} + \boldsymbol{h}^* e^{i\omega t}) \Bigg] \Bigg\} \\ = M_0 \mu_0 \Bigg[&\frac{-\hat{\boldsymbol{e}}_\varphi + i\hat{\boldsymbol{e}}_\vartheta}{(\omega_{\text{n}} - \omega)^2 + \frac{\alpha^2}{\eta^2}} \\ &\cdot \left(\frac{\omega_{\text{n}} - \omega}{\omega} \dot{\boldsymbol{H}}_{\text{osc}} + \frac{\alpha}{\eta} \boldsymbol{H}_{\text{osc}} \right) \Bigg]. \end{aligned} \tag{F1}$$

$\boldsymbol{T}_N$ can be approximated in the following way:

$$\boldsymbol{T}_N \approx \partial_t \Delta \boldsymbol{L}_N = -M_0 \mu_0 \left[\hat{\boldsymbol{e}}_\varphi \cdot \frac{(\omega_{\text{n}} - \omega)\omega \boldsymbol{H}_{\text{osc}} + \frac{\alpha}{\eta} \dot{\boldsymbol{H}}_{\text{osc}}}{(\omega_{\text{n}} - \omega)^2 + \frac{\alpha^2}{\eta^2}} \right] \hat{\boldsymbol{e}}_\vartheta \tag{F2}$$

$$+ M_0 \mu_0 \left[\hat{\boldsymbol{e}}_\vartheta \cdot \frac{(\omega_{\text{n}} - \omega)\omega \boldsymbol{H}_{\text{osc}} + \frac{\alpha}{\eta} \dot{\boldsymbol{H}}_{\text{osc}}}{(\omega_{\text{n}} - \omega)^2 + \frac{\alpha^2}{\eta^2}} \right] \hat{\boldsymbol{e}}_\varphi. \tag{F3}$$

Here we used the fact that $\ddot{\boldsymbol{H}}_{\text{osc}} = -\omega^2 \boldsymbol{H}_{\text{osc}}$, where $\boldsymbol{H}_{\text{osc}} = \boldsymbol{h} e^{-i\omega t} + \boldsymbol{h}^* e^{i\omega t}$ is the time-dependent oscillating field. Using Eq. (F1) and $\boldsymbol{N} = 2M_0 \cdot \hat{\boldsymbol{e}}_r$, we can write Eq. (12) in the limit where only the nutation term is kept on the right-hand side as

$$\begin{aligned} \boldsymbol{N} \times \ddot{\boldsymbol{N}} \approx &-2\gamma (M_0 \mu_0)^2 \left[\hat{\boldsymbol{e}}_\varphi \cdot \frac{\omega(\omega_{\text{n}} - \omega)\boldsymbol{H}_{\text{osc}} + \frac{\alpha}{\eta} \dot{\boldsymbol{H}}_{\text{osc}}}{(\omega_{\text{n}} - \omega)^2 + \frac{\alpha^2}{\eta^2}} \right] \\ &\times (\hat{\boldsymbol{e}}_\varphi \times \boldsymbol{H}_{\text{osc}}) \\ &- 2\gamma (M_0 \mu_0)^2 \left[\hat{\boldsymbol{e}}_\vartheta \cdot \frac{\omega(\omega_{\text{n}} - \omega)\boldsymbol{H}_{\text{osc}} + \frac{\alpha}{\eta} \dot{\boldsymbol{H}}_{\text{osc}}}{(\omega_{\text{n}} - \omega)^2 + \frac{\alpha^2}{\eta^2}} \right] \\ &\times (\hat{\boldsymbol{e}}_\vartheta \times \boldsymbol{H}_{\text{osc}}). \end{aligned} \tag{F4}$$

The projections of $\ddot{\boldsymbol{N}}$ on the $\hat{\boldsymbol{e}}_\vartheta$ and $\hat{\boldsymbol{e}}_\varphi$ directions are then given by Eqs. (14) and (15), respectively.

[1] C. D. Stanciu, F. Hansteen, A. V. Kimel, A. Kirilyuk, A. Tsukamoto, A. Itoh, and T. Rasing, All-Optical Magnetic Recording with Circularly Polarized Light, Phys. Rev. Lett. **99**, 047601 (2007).

[2] K. Vahaplar, A. M. Kalashnikova, A. V. Kimel, D. Hinzke, U. Nowak, R. Chantrell, A. Tsukamoto, A. Itoh, A. Kirilyuk, and T. Rasing, Ultrafast Path for Optical Magnetization Reversal via a Strongly Nonequilibrium State, Phys. Rev. Lett. **103**, 117201 (2009).

[3] I. Radu, K. Vahaplar, C. Stamm, T. Kachel, N. Pontius, H. A. Dürr, T. A. Ostler, J. Barker, R. F. L. Evans, R. W. Chantrell, A. Tsukamoto, A. Itoh, A. Kirilyuk, T. Rasing, and A. V. Kimel, Transient ferromagnetic-like state mediating ultrafast reversal of antiferromagnetically coupled spins, Nature (London) **472**, 205 (2011).

[4] K. Vahaplar, A. M. Kalashnikova, A. V. Kimel, S. Gerlach, D. Hinzke, U. Nowak, R. Chantrell, A. Tsukamoto, A. Itoh, A. Kirilyuk, and T. Rasing, All-optical magnetization reversal by circularly polarized laser pulses: Experiment and multiscale modeling, Phys. Rev. B **85**, 104402 (2012).

[5] M.-C. Ciornei, J. M. Rubí, and J.-E. Wegrowe, Magnetization dynamics in the inertial regime: Nutation predicted at short time scales, Phys. Rev. B **83**, 020410(R) (2011).

[6] J.-E. Wegrowe and M.-C. Ciornei, Magnetization dynamics, gyromagnetic relation, and inertial effects, Am. J. Phys. **80**, 607 (2012).

[7] D. Böttcher and J. Henk, Significance of nutation in magnetization dynamics of nanostructures, Phys. Rev. B **86**, 020404(R) (2012).

[8] R. Mondal, M. Berritta, A. K. Nandy, and P. M. Oppeneer, Relativistic theory of magnetic inertia in ultrafast spin dynamics, Phys. Rev. B **96**, 024425 (2017).

[9] E. Olive, Y. Lansac, M. Meyer, M. Hayoun, and J.-E. Wegrowe, Deviation from the Landau-Lifshitz-Gilbert equation in the inertial regime of the magnetization, J. Appl. Phys. **117**, 213904 (2015).

[10] E. Olive, Y. Lansac, and J.-E. Wegrowe, Beyond ferromagnetic resonance: The inertial regime of the magnetization, Appl. Phys. Lett. **100**, 192407 (2012).

[11] M. Cherkasskii, M. Farle, and A. Semisalova, Nutation resonance in ferromagnets, Phys. Rev. B **102**, 184432 (2020).

[12] R. Mondal, S. Großenbach, L. Rózsa, and U. Nowak, Nutation in antiferromagnetic resonance, Phys. Rev. B **103**, 104404 (2021).

[13] K. Neeraj, N. Awari, S. Kovalev, D. Polley, N. Zhou Hagström, S. S. P. K. Arekapudi, A. Semisalova, K. Lenz, B. Green, J.-C. Deinert, I. Ilyakov, M. Chen, M. Bawatna, V. Scalera, M. d'Aquino, C. Serpico, O. Hellwig, J.-E. Wegrowe, M. Gensch, and S. Bonetti, Inertial spin dynamics in ferromagnets, Nat. Phys. **17**, 245 (2021).

[14] S. Bhattacharjee, L. Nordström, and J. Fransson, Atomistic Spin Dynamic Method with both Damping and Moment of Inertia Effects Included from First Principles, Phys. Rev. Lett. **108**, 057204 (2012).

[15] Y. Li, A.-L. Barra, S. Auffret, U. Ebels, and W. E. Bailey, Inertial terms to magnetization dynamics in ferromagnetic thin films, Phys. Rev. B **92**, 140413(R) (2015).

[16] D. Thonig, O. Eriksson, and M. Pereiro, Magnetic moment of inertia within the torque-torque correlation model, Sci. Rep. **7**, 931 (2017).

[17] V. Unikandanunni, R. Medapalli, M. Asa, E. Albisetti, D. Petti, R. Bertacco, E. E. Fullerton, and S. Bonetti, Inertial spin dynamics in epitaxial cobalt films, arXiv:2109.03076 (2022).

[18] J. Mallinson, Damped gyromagnetic switching, IEEE Trans. Magn. **36**, 1976 (2000).

[19] G. Bertotti, I. Mayergoyz, C. Serpico, and M. Dimian, Comparison of analytical solutions of Landau–Lifshitz equation for damping and precessional switchings, J. Appl. Phys. **93**, 6811 (2003).

[20] T. Gilbert, A phenomenological theory of damping in ferromagnetic materials, IEEE Trans. Magn. **40**, 3443 (2004).

[21] T. Gerrits, H. A. M. van den Berg, J. Hohlfeld, L. Bär, and T. Rasing, Ultrafast precessional magnetization reversal by picosecond magnetic field pulse shaping, Nature (London) **418**, 509 (2002).

[22] S. Kaka and S. E. Russek, Precessional switching of submicrometer spin valves, Appl. Phys. Lett. **80**, 2958 (2002).

[23] I. Tudosa, C. Stamm, A. B. Kashuba, F. King, H. C. Siegmann, J. Stöhr, G. Ju, B. Lu, and D. Weller, The ultimate speed of magnetic switching in granular recording media, Nature (London) **428**, 831 (2004).

[24] A. V. Kimel, B. A. Ivanov, R. V. Pisarev, P. A. Usachev, A. Kirilyuk, and T. Rasing, Inertia-driven spin switching in antiferromagnets, Nat. Phys. **5**, 727 (2009).

[25] K. Neeraj, M. Pancaldi, V. Scalera, S. Perna, M. d'Aquino, C. Serpico, and S. Bonetti, Magnetization switching in the inertial regime, Phys. Rev. B **105**, 054415 (2022).

[26] See Supplemental Material at http://link.aps.org/supplemental/10.1103/PhysRevB.106.214403 for Supplemental Videos illustrating the switching processes in ferromagnets and in antiferromagnets.

[27] L. Rózsa, S. Selzer, T. Birk, U. Atxitia, and U. Nowak, Reduced thermal stability of antiferromagnetic nanostructures, Phys. Rev. B **100**, 064422 (2019).

[28] D. Polley, M. Pancaldi, M. Hudl, P. Vavassori, S. Urazhdin, and S. Bonetti, THz-driven demagnetization with perpendicular magnetic anisotropy: Towards ultrafast ballistic switching, J. Phys. D **51**, 084001 (2018).

[29] S. Sederberg, F. Kong, and P. B. Corkum, Tesla-Scale Terahertz Magnetic Impulses, Phys. Rev. X **10**, 011063 (2020).

[30] K. Jhuria, J. Hohlfeld, A. Pattabi, E. Martin, A. Y. Arriola Córdova, X. Shi, R. Lo Conte, S. Petit-Watelot, J. C. Rojas-Sanchez, G. Malinowski, S. Mangin, A. Lemaître, M. Hehn, J. Bokor, R. B. Wilson, and J. Gorchon, Spin–orbit torque switching of a ferromagnet with picosecond electrical pulses, Nat. Electron. **3**, 680 (2020).

[31] E. V. Gomonaĭ and V. M. Loktev, Distinctive effects of a spin-polarized current on the static and dynamic properties of an antiferromagnetic conductor, Low Temp. Phys. **34**, 198 (2008).